Article:
Nassar, AE and Mullis, AM orcid.org/0000-0002-5215-9959 (2021) Rapid screening of high-entropy alloys using neural networks and constituent elements. Computational Materials Science, 199. 110755. ISSN 0927-0256

https://doi.org/10.1016/j.commatsci.2021.110755

Rapid screening of High-Entropy Alloys using neural networks and constituent elements

A.E. Nassar and A.M. Mullis

School of Chemical and Process Engineering, University of Leeds, Leeds, LS2 9JT, UK

Abstract

Particularly over the past year, there has been a significant surge in machine learning (ML) methods to predict new High-Entropy Alloys (HEAs). Despite considerable achievements from these attempts, their models require datasets built on thermodynamic and Hume-Rothery (HR) features of the alloys. Often, some of these features are taxing to obtain and involve substantial estimations. Considering that an alloy's composition is always known for certain, we present the idea of using compositional (atomic percentage) data with a simple neural network to predict HEA phases. This is to encourage the use of ML and enable the average researcher to rapidly screen potential HEA compositions. We also explore a neural network which uses HR features along with the atomic percentage data and compare the two models. The neural network working with compositional data only (NN1) achieved an average testing accuracy of 92%, whereas the neural network working with HR features as well as compositional data (NN2) achieved an average testing accuracy of 90%. That NN1 outperforms the vast majority of models of the present date has significant implications, as it shows that the complete abandonment of predictive features is not only possible but also advantageous. To validate the models, we use NN1 and NN2 to predict the solid-solution window of the $Al_xCrCuFeNi$ system. Both networks predicts that beyond x = 1.4, the system is predominantly intermetallic. This was confirmed by arc-melting the x = 1.0, x = 1.3, x = 1.5 and x = 2 samples and studying their microstructures using SEM imaging.

Keywords: High-Entropy Alloys; Multi-Principal Element Alloys; Neural network; Phase prediction; Solidification microstructure.

1. Introduction

High-entropy alloys (HEAs) have attracted a great amount of academic attention over the past decade due to their vast potential applications. HEAs have come to be defined as multi-principal element alloys (MPEAs) with at least five elements all having equal, or near-equal, atomic ratios [1–4]. The consensus is also that HEAs form random single-phase solid solutions [5,6], although various dual-phase HEAs have been accepted [7–9]. Whether a HEA is single or dual-phase, the underlying lattices are generally high-symmetry, simple-solid solutions such as face-centered-cubic (FCC), body-centered-cubic (BCC) or hexagonal close-packed (HCP) [10]. The unexpected stability of these phases is thought to stem from the large configurational entropy of mixing ΔS_{mix} which reduces the Gibb's free energy of their solutions [11]. However, the exploration of HEAs remains, by and large, a trial and error process involving experiments which vary the atomic ratio of an element which is added to a base of elements already known to form an HEA [12,13]. As such, developing predictive models is extremely important in making the search for novel HEA compositions a more efficient process and in turn, allowing their integration into industrial and real-world applications to be accelerated.

Until 2017 most HEA prediction attempts involved a process of ensuring that simple thermodynamic and Hume-Rothery (HR) criteria are met [14,15]. More recently, attempts to employ machine learning (ML) methods (particularly neural networks) in predicting HEA phases [16–18] have been made. The biggest differentiator between neural networks and methods based on thermodynamic and/or HR features is that NNs do not utilise equations or analytical criteria to make predictions. Another unique aspect of NNs is their anticipated improvement in predictive capability as HEA databases grow. Efforts are also already being made in designing HEAs with desired properties using ML [19,20]. By using a database containing $Al_xCo_yCr_zCu_uFe_vNi_w$ HEAs and their hardness values to train a ML model, Wen *et al.* [21] reportedly managed to design HEAs with hardness values up to 10% higher than the largest value observed in the database. Apart from neural networks, several other ML models involving HEA phase prediction have been explored with the K^{th} nearest neighbor algorithm [22] and the random forest classification algorithm [23] attracting significant attention.

However, as ML models rely heavily on HEA databases, a foreseeable problem halting their progress is the lack of systematic recording of HEAs and their properties. For example, the impacts which processing methods have on an alloy's properties are often not considered when documenting HEAs. It is often the case that a given property of the same alloy can have two different reported values; these discrepancies are most likely attributed to differences in processing methods which have not been recorded. Some examples are the $AlCoCrCu_{0.5}FeNi$ alloy with hardness values reported to be 458HV, 563HV and 665HV [21], or the $Al_3FeNiCoCrCu$ alloy with a microstructure reported to be intermetallic (IM) [24] and solid-solution (SS) [25]. Generally, to achieve maximal results from a NN, the size of the data set should be as large as possible, with only alloys with high uncertainty being omitted. The data set used in this work finally included 391 alloys taken from references [24–26]. In order for the metallurgical community to make progress in ML to predict HEAs, HEA databases need to be put together with clear outlines of the processing techniques used to manufacture them.

The work presented within employs two neural networks, each with different input features. The first neural network (NN1) receives solely composition data as inputs. The second neural network (NN2) receives five input features in addition to the composition data which NN1 receives. These features are: entropy of mixing, enthalpy of mixing, valence electron concentration, atomic radius difference and Pauling electronegativity difference (ΔS_{mix}, ΔH_{mix}, VEC, δ and $\Delta\chi$ respectively). More precisely, the composition information used is atomic percentage. NN1 is designed with the motive that composition is essentially the only information which is known with high accuracy about an HEA, whereas all other possible input features (whether Hume-Rothery or thermodynamic) involve many estimates and calculations of averages. The inconsistency in the values of such parameters has been a pervasive issue until now and is often observed between databases or within the same database.

To highlight the need for our proposed model NN1 (which abandons all predictive parameters completely), considering the controversy around each parameter's relevance serves as a good example. Dongbo Dai et al. [27] show, using ML methods, that VEC to be the most important parameter in HEA phase prediction and ΔS_{mix} to be the least important, whereas in the ML-based study of Huang et al., δ is concluded to be the most relevant parameter [28]. Separate studies consistently conflict about the matter of parameter weightings, and this is further highlighted in a study by Zhang et al., where their use of ML with extended Miedema theory concludes that formation enthalpy and δ are the most relevant parameters in HEA prediction [29]. These are but a few examples that highlight the lack of unison within the field.

To outline another topic of controversy, Li et al. [30], Zhang et al. [31] and Zeng et al. [32] all show that using more than four predictive parameters results in diminishing returns on the testing accuracy of ML models. However, the model with highest reported testing accuracy today uses 13 features [33], outlining once more that the use predictive parameters inherently evokes a lack of coherency within the field. Otto et al. [34] had highlighted the shortcomings of HEA predictive parameters in 2013, in a study which outlined that MPEAs sharing similar HR values need not have the same resulting structures. The conclusions of this study certainly relate to the lack of consensus observed today. As such, we investigate the complete abandonment of these predictive parameters by using atomic percentage data only.

In this work, models NN1 and NN2 were used to predict the solid-solution window of the $Al_xCuCrFeNi$ quinary alloy. This alloy was chosen due to the lack of studies which have been carried out on it, coupled with interest in probing its phases. The neural network predicts that at the x =1.4 composition, the system transitions from solid-solution to intermetallic. To confirm this, the x = 1.0, x = 1.3, x = 1.5 and x = 2.0 compositions were manufactured. Studying the microstructures of these alloys using SEM, it was confirmed that the x = 1.5 alloy indeed contained a dominant intermetallic phase in comparison to the x = 1.0 and x =

1.3 compositions. This confirms the transition at $x = 1.4$. The $x = 2.0$ alloy was made to further confirm the presence of the intermetallic and explore its growth.

2. Methodology

2.1 Data compilation

The data on phases and HR features of the alloys was collected using references [24–26]. We expanded on these datasets by adding the composition data for each alloy. As such, a column dedicated to each element present in the database was initiated, with cells pertaining to absent elements in any given HEA being populated with an arbitrary, small number (-0.05 chosen in this work). These cells were not populated with zeros in order to avoid large error gradients in the weight calculations. Figure 1 shows a 5-row print of the data including composition as part of the input features. Finally, the output prediction from each of the models is either a 1 or a 0. The data was arranged such that a "1" correlates to a solid-solution (SS) or a SS with intermetallic (SS+IM). This choice was made as many accepted HEAs have minor IM phases and the orthodox definition that a HEA must strictly comprise a single-phase SS is evolving. In turn, a "0" signals an amorphous (AM) structure, an IM or (AM + IM). Although data in references [24–26] contained binary alloys, these were omitted in our work. However, our final database contained ternary alloys as well as MPEAs. Omitting the binary alloys was done in order to avoid their presence in the testing sets, which would lead to deceiving inflated accuracies. On the other hand, ternary alloys were retained as they aid the NN in developing connections between certain elements, yet are not as predictable as binaries. The data was shuffled to avoid the formation of patterns and bias and finally, feature scaling was implemented such that each instant in the column of a given HR parameter was divided by the maximum value in the column (see Equation 1). Feature scaling was not applied to composition columns, as maintaining the sum of each row to be around 100 and maintaining the constant arbitrary value of -0.05 influences the NN performance.

$$x_{i,new} = \frac{x_i}{x_{max}} \tag{1}$$

Where x_i is instance number i in feature x and x_{max} is the largest value in feature x. $x_{i,new}$ is the updated value of x_i.

	Alloy	Z	dH	dS	VEC	Ed	SS/IM	Al	Ni	Co	Cr	Fe	Cu	Ti	...
0	Al0.5CoCrCuFeNiTi1.4	0.59	0.51	0.58	0.69	0.42	0	7.25	14.49	14.49	14.49	14.49	14.49	20.29	
1	AlCoCrCu0.5FeNi2	0.44	0.66	0.35	0.76	0.33	1	15.38	30.77	15.38	15.38	15.38	7.69	-0.05	
2	Cu0.5NiCoCrAl0.5Fe2	0.34	0.78	0.32	0.78	0.28	1	8.33	16.67	16.67	16.67	33.33	8.33	-0.05	
3	Al0.5CrCuFeMnNi	0.39	0.82	0.42	0.76	0.39	1	9.09	18.18	-0.05	18.18	18.18	18.18	-0.05	
4	WNbMoTaV	0.25	0.75	0.24	0.39	0.94	1	-0.05	-0.05	-0.05	-0.05	-0.05	-0.05	-0.05	

Figure 1: 5-row print of the data set used in NN2. 'Z' denotes the difference in atomic radii and 'Ed' the difference in Pauling electronegativity. The SS/IM column indicates the HEA's phase, with 1 indicating (SS) or (SS+IM) and 0 indicating a (AM), (IM) or (AM+IM). Only 7 of the 37 elements present in the database are shown. A small arbitrary value (-0.05) was chosen to indicate the absence of an element.

2.3 Neural networks

Figures 2a and 2b shows a schematic of the architectures used for NN1 and NN2, respectively. The neural networks were constructed using the Keras API in the Google Collaboratory environment, with the Pandas library used to import the final data set of 391 alloys. A 70/30 split was used between the training and

testing data respectively for each of the NNs. To assess the average prediction accuracies of the neural networks the data was shuffled and fed back to the models three times. Choosing the right hyperparameters for the neural networks is of vital importance in maximising their performance. NN1 (neural network including elemental composition data only) is the main focus of this work as it uses a dataset which, to the best of the authors' knowledge, has not been used to this scale before. The optimal hyperparameters for NN1 were found to be: learning rate = 0.3, batch size = 3, number of hidden layers = 9 and the maximum number of units in a hidden layer = 192. The input dimension for NN1 is 37, in accordance with the number of elements in the database, while the output layer comprises 1 unit. Each of the above parameters was chosen as the best value by iterating through a pre-defined range. For instance, in determining the best learning rate, a range of values from 0.1 to 1 were probed, with the value leading to best predictive accuracy being chosen.

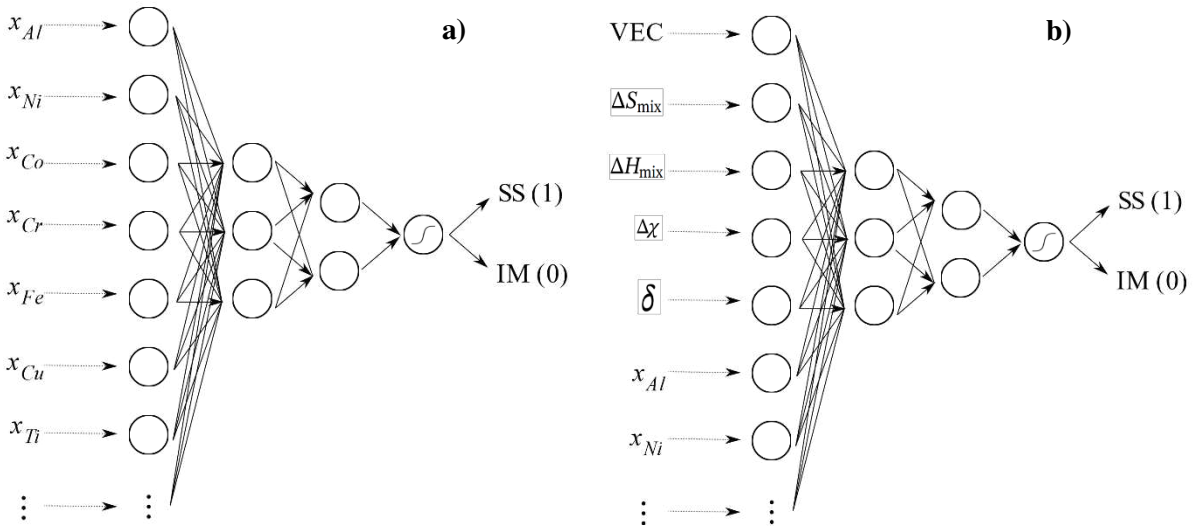

Figure 2a: – Schematics of NN1 and **b:** NN2 architectures. Number of hidden layers and number of units per layer shown are not representative of the true models but help in visualising the networks. The output layer in both architectures is shown as a Sigmoid activation function with binary output.

The activation function chosen for the hidden layers was the Rectified Linear Unit (ReLU) activation function, as it yielded the best results when compared to other activation functions. The ReLU activation function maintains the value being passed to a unit in the hidden layer unless the value is negative, in which case the value is made equal to zero [35] (see Figure 3a). This simple calculation keeps its computational cost to a minimum making it a very frequently used function. For the output layer the logarithmic sigmoid (logsig) activation function was used as this generates outputs of either 0 or 1 (see Figure 3b). As the NN is classifying binary features, this is the optimal activation function for this purpose.

The sigmoid activation function is described as per Equation 2 [36].

$$S(x) = \frac{1}{1 + e^{-x}} \tag{2}$$

Where x is any input value which is forced to a zero or one output denoted as $S(x)$.

To predict the phase of a previously uninvestigated HEA using the NNs designed in this work, the HEA's five features (ΔS_{mix}, ΔH_{mix}, VEC, δ and $\Delta\chi$) must first be calculated, allowing the HEA to be added to the database. The atomic percentages of the alloy's elements must also be calculated in a manner that is

consistent with the database. Upon adding the HEA to the database, the cell indicating the HEA's phase can be randomly chosen (0 or 1), as this will not affect the NN's prediction. The HEA of unknown phase is then intentionally made to be the only alloy in the "testing set", as the rest of the alloys (all 391) in this case are used in the training set to enhance the NN's learning. In this work, this process was applied for the $Al_xCuCrFeNi$ alloys, yielding predictions which were verified.

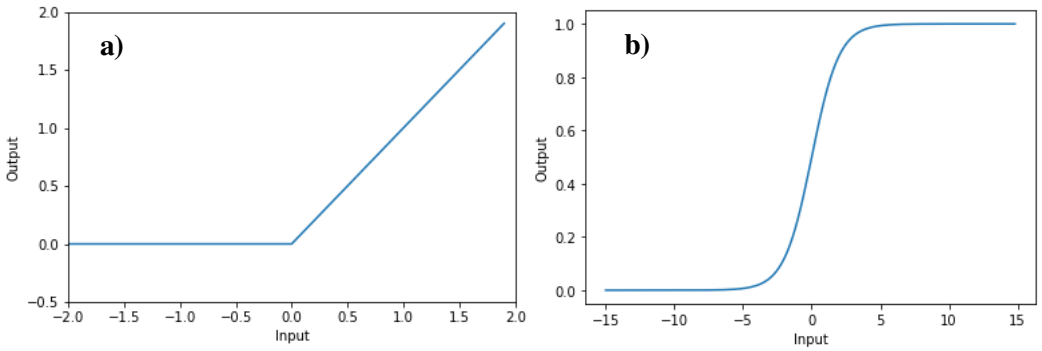

Figure 3a: Rectified Linear Unit and **b:** Sigmoid activation functions.

2.4 Alloy fabrication

The ingots were prepared using an arc-melter with a water-cooled copper hearth and a current of 230 Amp. For each of the alloy, aluminium and copper were first melted together in a high-vacuum furnace to avoid the formation of aluminium oxide. The remaining elements were then progressively added to the Al-Cu binary using the arc-melter. The arc-melter's vacuum chamber was purged with Argon four times before each melt. As the final alloy was reached by progressively adding elements to the Al-Cu binaries, all the intermediate alloys as well as the final alloy were turned over and melted four times to ensure homogeneity. Each of the constituent elements had a purity of > 99.9 wt%.

2.5 Sample analysis

The ingots obtained from the arc-melter were hot mounted using Phenolic resin and grounded using abrasive SiC paper down to the P2500 size. The mounted alloy was then automatically polished using Colloidal Silica and etched with aqua regia for 15 seconds to be observed under a Hitachi SU8230 scanning electron microscope (SEM). The SEM was used in backscattered electron detection mode to examine the microstructures of the samples.

3 Results and discussion

3.1 Neural networks

To accurately assess the neural networks in this work, the original dataset was shuffled and refed to the NNs three times. This ensures that alloy systems which are easier to predict do not consistently appear in the testing set, inflating the accuracy. Such systems may be tertiary alloys or HEAs which share the same base of elements and differing only slightly in composition. Figures 4 and 5 show the accuracy and loss of NN1 and NN2, respectively, for three different runs between which the data was shuffled. It is important to ensure that the NN's performance is not affected by data shuffling as this confirms that its results are reproducible with other data sets and that its predictions are scalable as the dataset grows. The accuracy the NN achieves in the test set (set of data the neural networks had not been exposed to before) is recorded after each run, with the average accuracy of the three runs taken to be the representative value of the NN's

accuracy. A NN's accuracy in the test set is calculated by finding the number of correctly predicted instances as a percentage of the total number of instances in the training set.

For predictions on the testing set, NN1 and NN2 achieved average accuracies of 92% and 90%, respectively. To further confirm the advantage of introducing compositional information to the dataset, a third NN operating only on HR features was also implemented and found to achieve a testing accuracy of 81%. To the best of the authors' knowledge, the only model which exceeds the performance of NN1 was implemented by Lee et al. [33], which achieved a testing accuracy value of 93%. Considering that this model uses 13 predictive features and a generative adversarial framework, NN1 appears to retain the aforementioned advantage of simplicity and scalability. That NN1 achieves a testing accuracy of 92% has significant implications, as it shows that the complete abandonment of predictive parameters is not only possible but also advantageous. This result comes as no surprise, since atomic percentage data does not require estimations to be made (unlike thermodynamic and HR features), hence leading to datasets that are more consistent and less prone to errors. Although vast efforts have been expended on modifying

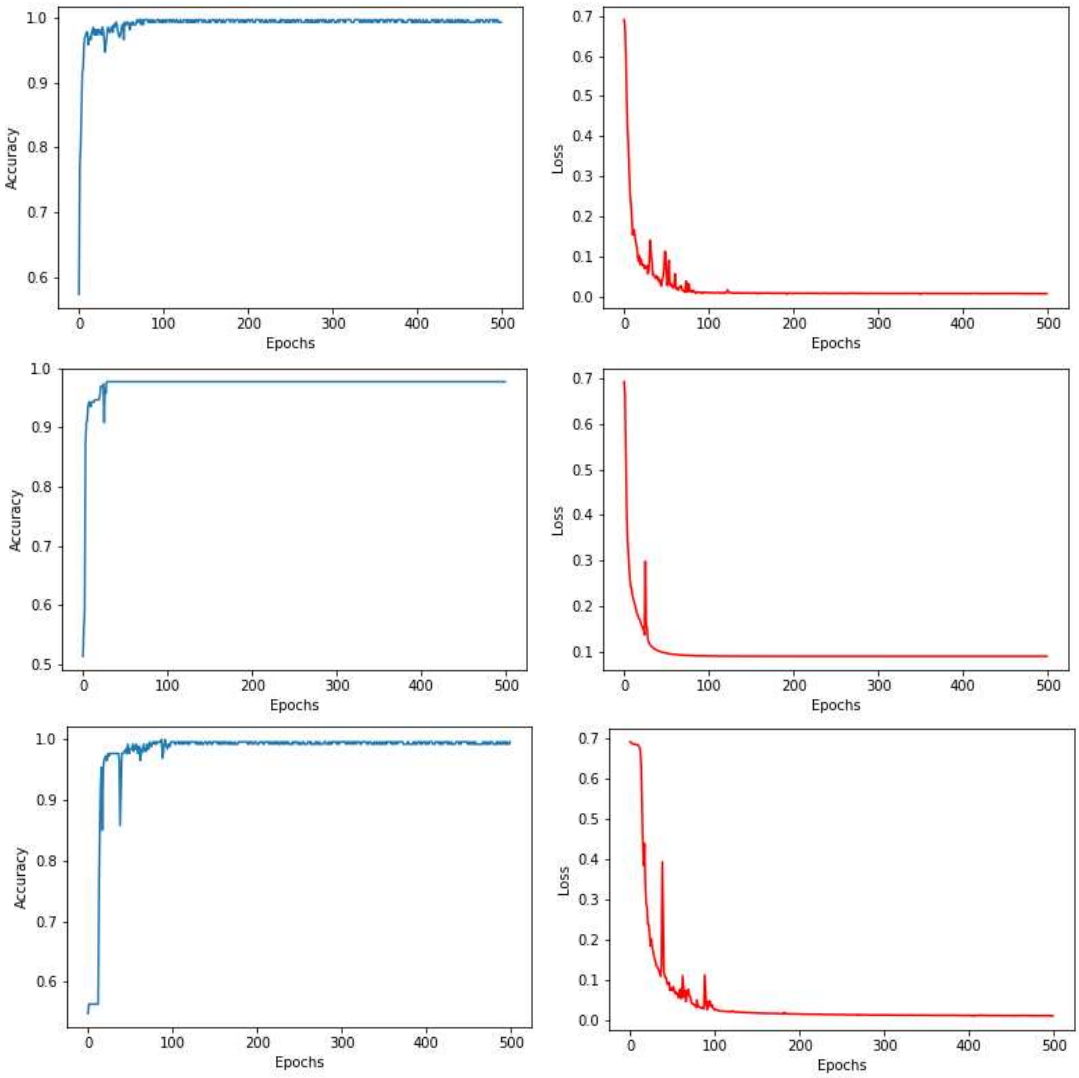

Figure 4: – Training loss and accuracy for NN1. Between each set of plots, the data is shuffled and 70% of the data is taken for training.

thermodynamic and HR parameters to capture finer phenomenological details [37–40], the saturation in the number of parameters has become evident and the field is in need of a leaner approach.

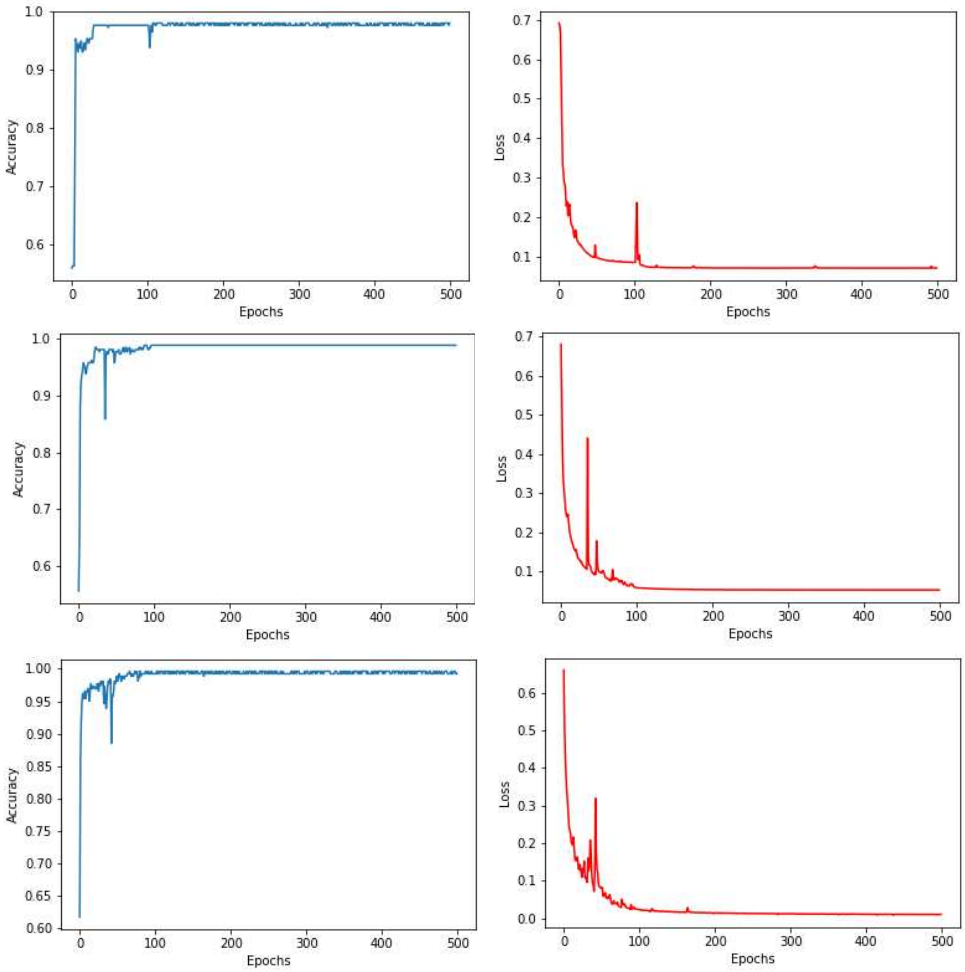

Figure 5: – Training loss and accuracy for NN2. Between each set of plots, the data is shuffled and 70% of the data is taken for training.

3.2. Microstructure analysis

According to the NNs designed in this work, $x = 1.4$ is the composition in the $Al_xCuCrFeNi$ system at which the output changes from "1" to "0" as x increases. As such, the compositions directly above and below this point were chosen to be manufactured ($x = 1.3$ and $x = 1.5$), as well as compositions further away from this critical point ($x = 1.0$ and $x = 2.0$). In total, four alloys from the $Al_xCuCrFeNi$ system are fabricated using a combination of high-vacuum furnace and arc-melting. The $x = 1.0$ and $x = 1.3$ compositions corresponded to "1" in binary, indicating SS or (SS+IM) structures, whereas the $x = 1.5$ and $x = 2.0$ compositions corresponded to "0" in binary, indicating AM, IM or (AM +IM) structures.

The microstructure of the $x = 1.0$ alloy can be seen in Figure 6a, where a predominantly dendritic structure is evident. A minor phase is present in the matrix however and is more visible at the higher magnification in Figure 5b. This IM has been previously characterised as $AlFe_{0.23}Ni_{0.77}$ with a volume fraction reported to be 18% (obtained via XRD peak intensity analysis) [41]. Its reported B2 structure confirms that it is likely to be the Al-Ni phase in which Fe substitutes Ni. The $x = 1.3$ alloy displays a very similar morphology (see Figure 7a), where the needle-like intermetallic remains within the dendrites' vicinity but extends further outwards than what is observed in the $x = 1.0$ microstructure (see Figure 7b). Observing the fine (nano-scale) precipitates within the dendrites of both alloys, it is likely that they have formed via spinodal decomposition. Comparing these microstructures with some of the single-phase solid-solution HEAs (e.g. Cantor alloy – CoCrFeMnNi), it can be argued that they display overly complex morphologies to be classified as HEAs. However, many multi-phase alloys have been reported over the last decade that have been widely accepted as HEAs [42–44], as long as the behavior of the MPEA is consistent with HEA properties. Since such MPEAs have been classified as HEAs comprising (SS+IM) structures and encoded as "1" entries in the datasets, it is fully expected that the $x = 1.0$ and $x = 1.3$ compositions be predicted accordingly.

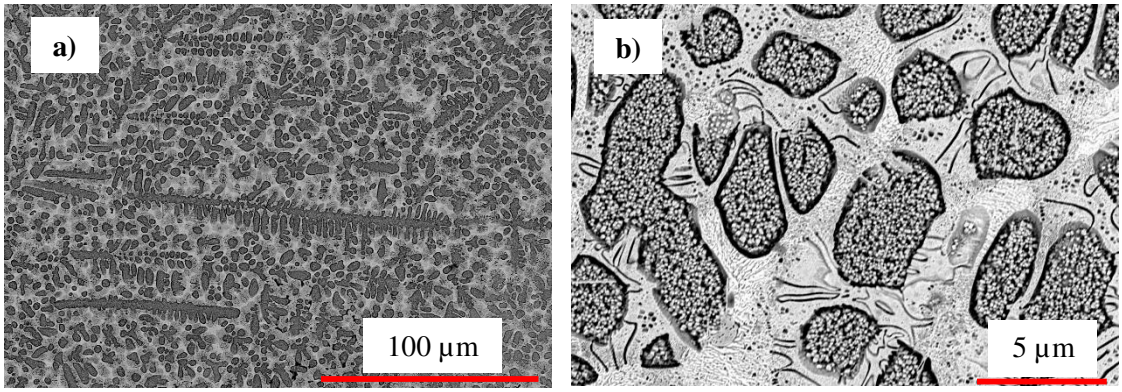

Figure 6a: – Micrograph of $Al_{1.0}CrCuFeNi$ showing dendritic structure **b:** Appearance of needle-like IM only observable at higher magnifications.

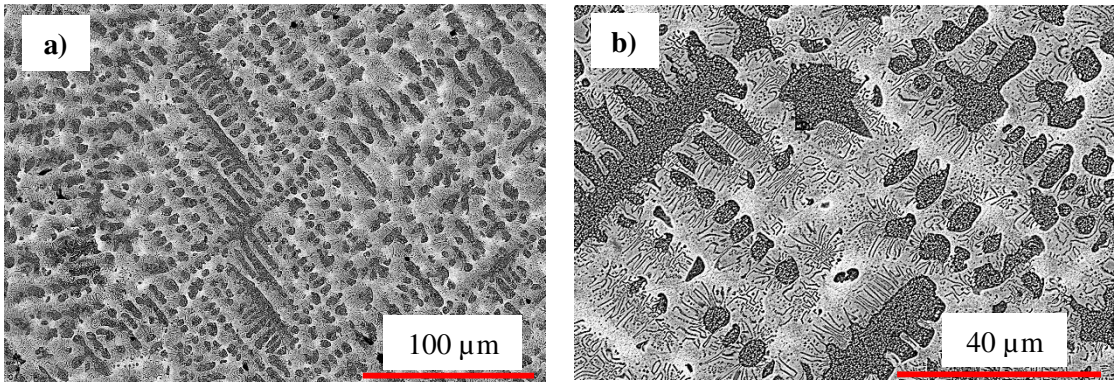

Figure 7a: – Micrograph of $Al_{1.3}CrCuFeNi$ showing dendritic structure **b:** higher magnification micrograph of $Al_{1.3}CrCuFeNi$, showing increased presence of IM phase relative to the $x = 1.0$ composition

The $x = 1.5$ alloy was found to comprise two unique features in its microstructure (both which confirm its classification as an alloy with dominant IM phases). The first feature, shown in Figure 8a, is the morphology of the IM phase forming a structure commonly referred to as "Chinese script" [45,46]. Unlike the $x = 1.0$ and $x = 1.3$ alloys, the IM phase here does not adhere to the local vicinity of the dendrites. Rather, the IM phase forms a Chinese script structure extending into the matrix. The second feature in this alloy (seen in

Figure 8b) has been observed previously in $Al_2CrCuFeNi_2$, where it is referred to as a "sunflower" structure [47]. In this work, Guo et al. classify the petals of the sunflower structure to be a eutectic of a Ni-Al-rich B2 phase and a Cr-rich BCC phase. The internal section of the structure is considered to be where the primary B2 phase originates from and within this region, fine BCC precipitates form as a result of spinodal decomposition. Finally, the needle-like IM observed in the $x = 1.0$ and $x = 1.3$ compositions is still present at the vicinity of the dendrites.

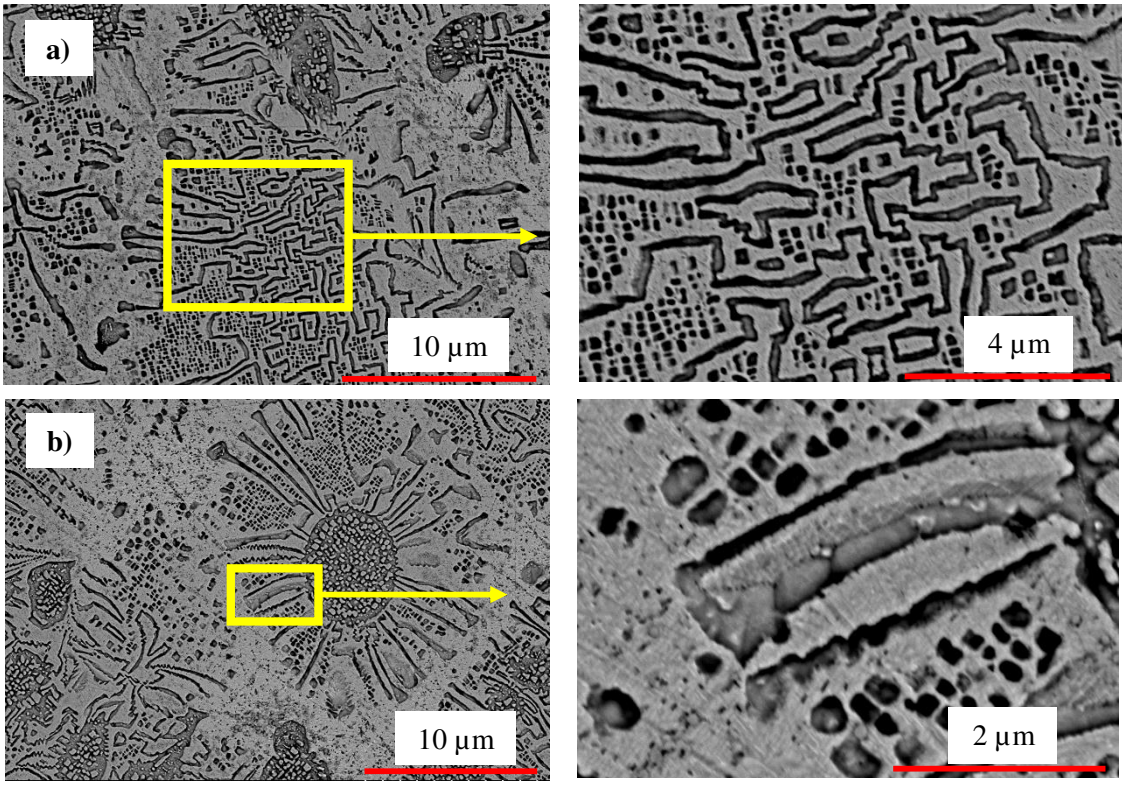

Figure 8a: – Micrograph of $Al_{1.5}CrCuFeNi$ showing "Chinese script" IM structure in the matrix at low magnification (left) and high magnification (right) **b:** "Sunflower" structure in $Al_{1.5}CrCuFeNi$ showing matrix dominated by intermetallics (left) and higher magnification focusing on lamellar region (right).

The $Al_2CrCuFeNi$ alloy has a brittle nature that is notably reflected in its mechanical behavior. Figure 9a shows a visible collection of micro-cracks in the surface morphology of the alloy. It is important to note that the cracks shown were not intentionally induced via mechanical operations, but rather as a result of handling of the alloy in standard processes such as mounting, cutting etc. Such cracks further confirm that the prediction made by the models is correct and that the $Al_2CuCrFeNi$ alloy comprises excessive dominance of IM phases in its microstructure. Figure 9b shows an SEM micrograph of $Al_2CuCrFeNi$, outlining the presence of coarse spherical precipitates in the interdendritic region, together with much finer spherical and needle shaped precipitates decorating the dendrite boundaries. Although the exact structures of the observed IM phases have not been identified, the study of their morphologies is not the primary objective of this work – the focus within is to confirm the application of the presented rapid-screening method. However, the extremely brittle nature of the alloy indicates that these dominant IM phases are A2/B2 precipitates, as these phases take away from the alloy's ductility and have been shown to grow with increasing aluminium content in alloys such as $Al_xCoCrFeMnNi$ [48].

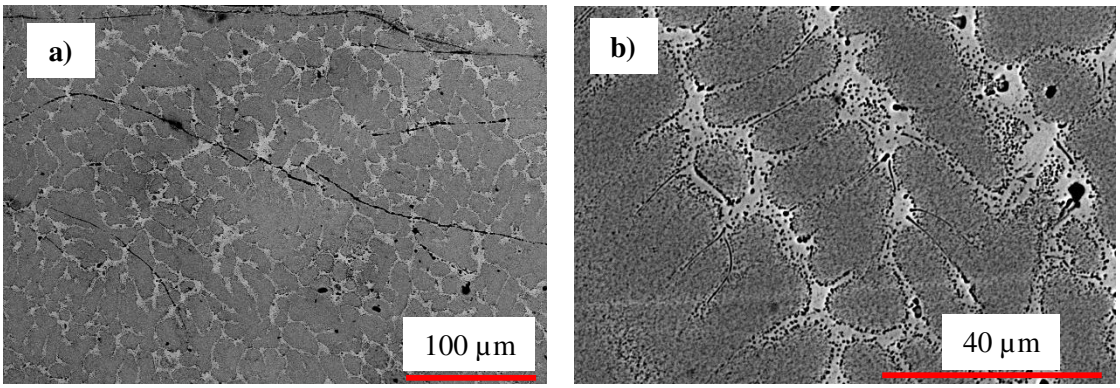

Figure 8a: – Micro-cracks in microstructure of $Al_{2.0}$CrCuFeNi outlining the brittle nature of the alloy **b:** Overall microstructure of $Al_{2.0}$CrCuFeNi showing coarse sphere-like and needle intermetallics in its matrix.

4 Conclusions

In this study, two models were designed to predict HEA phases. The first model – a neural network referred to throughout the work as NN1 – operated with a dataset including atomic percentage data only and yielded an average prediction accuracy of 92%. The second model, NN2, used a dataset including HR features as well as atomic percentage data. NN2 yielded an average prediction accuracy of 90%. The HR features added to the database for NN2 are ΔS_{mix}, ΔH_{mix}, VEC, δ and $\Delta\chi$.

As far as the authors are aware, the predictive accuracy of NN1 is only 1% less than the highest accuracy achieved by researchers to date. The fact that NN1 performs with such accuracy has significant implications as it shows that the complete abandonment of predictive features is not only possible but also advantageous. This result comes as no surprise, since atomic percentage data does not require estimations to be made (unlike thermodynamic and HR features), thus leading to datasets that are more consistent and less prone to errors. Due to the current saturation in the number of predictive parameters, a lean and accurate approach such as that of NN1 is crucial in achieving models that are scalable for rapid use by researchers.

NN1 and NN2 were used to predict the limit of the SS in the Al_xCuCrFeNi system, yielding the prediction that at x = 1.4 the system transitions from a SS/SS+IM to an IM/AM. The x = 1.0, x = 1.3, x = 1.5 and x = 2.0 alloys were manufactured using an arc-melter to confirm the predictions obtained from the models NN1 and NN2. The x = 1.0 and x = 1.3 compositions were confirmed to comprise SS+IM microstructures with the IM phase adhering to the vicinity of the dendrites.

The x = 1.5 system showed a significantly more complex microstructure, in which a "Chinese script" IM was observed in addition to a "sunflower structure" comprising a lamellar eutectic surrounding nano-scale preciptates appearing to have formed via spinodal decomposition. As such, the prediction of NN1 and NN2 is justified upon observing the complexity of the x = 1.5 micrographs. Finally, the x = 2 composition (which was manufactured to confirm IM saturation as x is increased) yields an alloy that is very brittle in nature and a microstructure showing the clear presence of coarse spherical IM precipitates in the interdendritic region, together with much finer spherical and needle shaped precipitates decorating the dendrite boundaries.

Acknowledgements

This research was funded by EPSRC Innovative Manufacturing Research Hub in Liquid Metal Engineering (LiME), Grant No. EP/N007638/1.

References

[1] D.B. Miracle, O.N. Senkov, A critical review of high entropy alloys and related concepts, Acta Mater. (2017). https://doi.org/10.1016/j.actamat.2016.08.081.

[2] B. Cantor, Multicomponent and high entropy alloys, Entropy. 16 (2014) 4749–4768. https://doi.org/10.3390/e16094749.

[3] B.S. Murty, J.W. Yeh, S. Ranganathan, P.P. Bhattacharjee, A brief history of alloys and the birth of high-entropy alloys, in: High-Entropy Alloy., 2019. https://doi.org/10.1016/b978-0-12-816067-1.00001-1.

[4] B. Cantor, Multicomponent high-entropy Cantor alloys, Prog. Mater. Sci. (2021). https://doi.org/10.1016/j.pmatsci.2020.100754.

[5] Y. Zhang, History of High-Entropy Materials, in: High-Entropy Mater., 2019. https://doi.org/10.1007/978-981-13-8526-1_1.

[6] B.S. Murty, J.W. Yeh, S. Ranganathan, A Brief History of Alloys and the Birth of High-Entropy Alloys, in: High Entropy Alloy., 2014. https://doi.org/10.1016/b978-0-12-800251-3.00001-8.

[7] N. Haghdadi, S. Primig, M. Annasamy, P. Cizek, P.D. Hodgson, D.M. Fabijanic, Dynamic recrystallization in AlXCoCrFeNi duplex high entropy alloys, J. Alloys Compd. (2020). https://doi.org/10.1016/j.jallcom.2020.154720.

[8] H. Zheng, R. Chen, G. Qin, X. Li, Y. Su, H. Ding, J. Guo, H. Fu, Phase separation of AlCoCrFeNi2.1 eutectic high-entropy alloy during directional solidification and their effect on tensile properties, Intermetallics. 113 (2019). https://doi.org/10.1016/j.intermet.2019.106569.

[9] A. Shafiei, Design of Eutectic High Entropy Alloys in Al–Co–Cr–Fe–Ni System, Met. Mater. Int. (2021). https://doi.org/10.1007/s12540-020-00655-3.

[10] M.H. Tsai, J.W. Yeh, High-entropy alloys: A critical review, Mater. Res. Lett. 2 (2014) 107–123. https://doi.org/10.1080/21663831.2014.912690.

[11] Y.F. Ye, Q. Wang, Y.L. Zhao, Q.F. He, J. Lu, Y. Yang, Elemental segregation in solid-solution high-entropy alloys: Experiments and modeling, J. Alloys Compd. (2016). https://doi.org/10.1016/j.jallcom.2016.04.239.

[12] J.W. Yeh, Alloy design strategies and future trends in high-entropy alloys, Jom. 65 (2013) 1759–1771. https://doi.org/10.1007/s11837-013-0761-6.

[13] H. Jiang, K. Han, X. Gao, Y. Lu, Z. Cao, M.C. Gao, J.A. Hawk, T. Li, A new strategy to design eutectic high-entropy alloys using simple mixture method, Mater. Des. 142 (2018) 101–105. https://doi.org/10.1016/j.matdes.2018.01.025.

[14] N. Guo, X. Gao, L. Wang, G. Zhu, Phase Formation Rules and Design Methods of High-entropy Alloys, Tezhong Zhuzao Ji Youse Hejin/Special Cast. Nonferrous Alloy. (2019). https://doi.org/10.15980/j.tzzz.2019.10.008.

[15] W. Yu, Y. Qu, C. Li, Z. Li, Y. Zhang, Y. Guo, J. You, R. Su, Phase selection and mechanical properties of (Al 21.7 Cr 15.8 Fe 28.6 Ni 33.9) x (Al 9.4 Cr 19.7 Fe 41.4 Ni 29.5) 100-x high entropy alloys, Mater. Sci. Eng. A. (2019). https://doi.org/10.1016/j.msea.2019.02.067.

[16] N. Islam, W. Huang, H.L. Zhuang, Machine learning for phase selection in multi-principal element alloys, Comput. Mater. Sci. 150 (2018) 230–235. https://doi.org/10.1016/j.commatsci.2018.04.003.

[17] B. Debnath, A. Vinoth, M. Mukherjee, S. Datta, Designing Fe-based high entropy alloy-a machine learning approach, in: IOP Conf. Ser. Mater. Sci. Eng., 2020. https://doi.org/10.1088/1757-899X/912/5/052021.

[18] A. Roy, G. Balasubramanian, Predictive descriptors in machine learning and data-enabled explorations of high-entropy alloys, Comput. Mater. Sci. (2021). https://doi.org/10.1016/j.commatsci.2021.110381.

[19] Y.J. Chang, C.Y. Jui, W.J. Lee, A.C. Yeh, Prediction of the Composition and Hardness of High-Entropy Alloys by Machine Learning, Jom. 71 (2019) 3433–3442. https://doi.org/10.1007/s11837-019-03704-4.

[20] L. Li, B. Xie, Q. Fang, J. Li, Machine Learning Approach to Design High Entropy Alloys with Heterogeneous Grain Structures, Metall. Mater. Trans. A Phys. Metall. Mater. Sci. (2021). https://doi.org/10.1007/s11661-020-06099-z.

[21] C. Wen, Y. Zhang, C. Wang, D. Xue, Y. Bai, S. Antonov, L. Dai, T. Lookman, Y. Su, Machine learning assisted design of high entropy alloys with desired property, Acta Mater. 170 (2019) 109–117. https://doi.org/10.1016/j.actamat.2019.03.010.

[22] R. Machaka, Machine Learning Based Prediction of Phases in High-Entropy Alloys, SSRN Electron. J. (2020). https://doi.org/10.2139/ssrn.3530328.

[23] U. Bhandari, M.R. Rafi, C. Zhang, S. Yang, Yield strength prediction of high-entropy alloys using machine learning, Mater. Today Commun. (2021). https://doi.org/10.1016/j.mtcomm.2020.101871.

[24] Y.F. Ye, Q. Wang, J. Lu, C.T. Liu, Y. Yang, High-entropy alloy: challenges and prospects, Mater. Today. 19 (2016) 349–362. https://doi.org/10.1016/j.mattod.2015.11.026.

[25] S. Guo, C.T. Liu, Phase stability in high entropy alloys: Formation of solid-solution phase or amorphous phase, Prog. Nat. Sci. Mater. Int. 21 (2011) 433–446. https://doi.org/10.1016/S1002-0071(12)60080-X.

[26] K. Kaufmann, K.S. Vecchio, Searching for high entropy alloys: A machine learning approach, Acta Mater. (2020). https://doi.org/10.1016/j.actamat.2020.07.065.

[27] D. Dai, T. Xu, X. Wei, G. Ding, Y. Xu, J. Zhang, H. Zhang, Using machine learning and feature engineering to characterize limited material datasets of high-entropy alloys, Comput. Mater. Sci. (2020). https://doi.org/10.1016/j.commatsci.2020.109618.

[28] W. Huang, P. Martin, H.L. Zhuang, Machine-learning phase prediction of high-entropy alloys, Acta Mater. 169 (2019) 225–236. https://doi.org/10.1016/j.actamat.2019.03.012.

[29] L. Zhang, H. Chen, X. Tao, H. Cai, J. Liu, Y. Ouyang, Q. Peng, Y. Du, Machine learning reveals the importance of the formation enthalpy and atom-size difference in forming phases of high entropy alloys, Mater. Des. (2020). https://doi.org/10.1016/j.matdes.2020.108835.

[30] Y. Li, W. Guo, Machine-learning model for predicting phase formations of high-entropy alloys, Phys. Rev. Mater. (2019). https://doi.org/10.1103/PhysRevMaterials.3.095005.

[31] Y. Zhang, C. Wen, C. Wang, S. Antonov, D. Xue, Y. Bai, Y. Su, Phase prediction in high entropy alloys with a rational selection of materials descriptors and machine learning models, Acta Mater. 185 (2020) 528–539. https://doi.org/10.1016/j.actamat.2019.11.067.

[32] Y. Zeng, M. Man, K. Bai, Y.W. Zhang, Revealing high-fidelity phase selection rules for high

entropy alloys: A combined CALPHAD and machine learning study, Mater. Des. (2021). https://doi.org/10.1016/j.matdes.2021.109532.

[33] S.Y. Lee, S. Byeon, H.S. Kim, H. Jin, S. Lee, Deep learning-based phase prediction of high-entropy alloys: Optimization, generation, and explanation, Mater. Des. (2021). https://doi.org/10.1016/j.matdes.2020.109260.

[34] F. Otto, Y. Yang, H. Bei, E.P. George, Relative effects of enthalpy and entropy on the phase stability of equiatomic high-entropy alloys, Acta Mater. 61 (2013) 2628–2638. https://doi.org/10.1016/j.actamat.2013.01.042.

[35] F. Ertam, Data classification with deep learning using tensorflow, in: 2nd Int. Conf. Comput. Sci. Eng. UBMK 2017, 2017: pp. 755–758. https://doi.org/10.1109/UBMK.2017.8093521.

[36] F. Nelli, Deep Learning with TensorFlow, in: Python Data Anal., 2018: pp. 349–407. https://doi.org/10.1007/978-1-4842-3913-1_9.

[37] Y.F. Ye, Q. Wang, J. Lu, C.T. Liu, Y. Yang, Design of high entropy alloys: A single-parameter thermodynamic rule, Scr. Mater. 104 (2015) 53–55. https://doi.org/10.1016/j.scriptamat.2015.03.023.

[38] M. Zheng, W. Ding, W. Cao, S. Hu, Q. Huang, A quick screening approach for design of multi-principal element alloy with solid solution phase, Mater. Des. (2019). https://doi.org/10.1016/j.matdes.2019.107882.

[39] Y.F. Ye, Q. Wang, J. Lu, C.T. Liu, Y. Yang, The generalized thermodynamic rule for phase selection in multicomponent alloys, Intermetallics. (2015). https://doi.org/10.1016/j.intermet.2014.12.011.

[40] O.N. Senkov, D.B. Miracle, A new thermodynamic parameter to predict formation of solid solution or intermetallic phases in high entropy alloys, J. Alloys Compd. (2016). https://doi.org/10.1016/j.jallcom.2015.10.279.

[41] P. Jinhong, P. Ye, Z. Hui, Z. Lu, Microstructure and properties of AlCrFeCuNi x ($0.6 \leq x \leq 1.4$) high-entropy alloys, Mater. Sci. Eng. A. (2012). https://doi.org/10.1016/j.msea.2011.11.063.

[42] A.M. Manzoni, S. Haas, H. Daoud, U. Glatzel, C. Förster, N. Wanderka, Tensile behavior and evolution of the phases in the Al10Co25Cr8Fe15Ni36Ti6 compositionally complex/high entropy alloy, Entropy. (2018). https://doi.org/10.3390/e20090646.

[43] N. Derimow, R. Abbaschian, Liquid phase separation in high-entropy alloys-a review, Entropy. (2018). https://doi.org/10.3390/e20110890.

[44] F. Müller, B. Gorr, H.J. Christ, H. Chen, A. Kauffmann, S. Laube, M. Heilmaier, Formation of complex intermetallic phases in novel refractory high-entropy alloys NbMoCrTiAl and TaMoCrTiAl: Thermodynamic assessment and experimental validation, J. Alloys Compd. (2020). https://doi.org/10.1016/j.jallcom.2020.155726.

[45] G. Yuan, M. Liu, Q. Wang, Y. Zhu, W. Ding, Microstructure refinement of Mg-Al-Zn-Si alloys, Jinshu Xuebao/Acta Metall. Sin. (2002).

[46] J.Y. Hwang, H.W. Doty, M.J. Kaufman, The effects of Mn additions on the microstructure and mechanical properties of Al-Si-Cu casting alloys, Mater. Sci. Eng. A. (2008). https://doi.org/10.1016/j.msea.2007.12.026.

[47] S. Guo, C. Ng, C.T. Liu, Sunflower-like solidification microstructure in a near-eutectic high-

entropy alloy, Mater. Res. Lett. (2013). https://doi.org/10.1080/21663831.2013.844737.

[48] C.J. Tong, Y.L. Chen, S.K. Chen, J.W. Yeh, T.T. Shun, C.H. Tsau, S.J. Lin, S.Y. Chang, Microstructure characterization of AlxCoCrCuFeNi high-entropy alloy system with multiprincipal elements, Metall. Mater. Trans. A Phys. Metall. Mater. Sci. 36 (2005) 881–893. https://doi.org/10.1007/s11661-005-0283-0.